JOURNAL OF MATERIALS SCIENCE 19 (1984) 245–253

Temperature dependence of friction force acting on dislocations in silicon crystals

YOICHI NISHINO, HIROYASU SAKA, TORU IMURA
Department of Crystalline Materials Science and Department of Metallurgy, Faculty of Engineering, Nagoya University, Chikusa-ku Nagoya 464, Japan

The characteristics of the dislocation motion in silicon crystals during annealing have been investigated by means of *in situ* X-ray topographic observations in the temperature range from 1173 to 1273 K. When annealed at elevated temperatures, the small displacements in position of the dislocation segments took place so as to balance the friction force acting on these segments with the elastic interaction force between dislocations. From the analysis of (i) repulsive interaction between parallel screw dislocations with the same sign, and of (ii) configurational changes of dislocation half-loops, the friction force acting on dislocations can be determined at each annealing temperature by estimating the repulsive interaction force between parallel dislocations, and the force due to line tension for curved dislocation. On the basis of the analysis of the temperature dependence of friction force, the activation energy for dislocation motion is evaluated to be 2.4 eV for a screw dislocation and 2.2 eV for a 60° dislocation.

1. Introduction

Silicon crystal is a typical crystalline material in which the Peierls–Nabarro barrier for dislocation motion is extremely large because of the covalent bonding [1]. In such a crystal, thermal fluctuations assist the applied stress in letting a dislocation past the barrier. It has been shown by X-ray topography that the mobility of dislocations in silicon crystals is much lower than those in other types of crystals and that the dislocation velocity is sensitive to temperature but rather insensitive to stress [2–7]. The dislocation velocity in silicon crystals is expressed approximately by the equation

$$v = B_0 \tau^m \exp(-E/kt) \quad (1)$$

where τ is the applied shear stress, T the temperature, k the Boltzmann constant, and B_0 a constant. According to the *in situ* X-ray topographic observations [7, 8], the magnitudes of activation energy E are estimated to be 2.1 ± 0.1 eV for a screw dislocation and 2.2 ± 0.15 eV for a 60° dislocation, and the magnitude of m is 1.1 ± 0.1 for both types of dislocations. It has been also disclosed that dislocations in float-zone crystals move at velocities given by Equation 1 under applied stresses above 1.5 MN m^{-2} [7, 8].

It is known that expanded dislocation half-loops shrink during annealing at elevated temperatures [9–11], and that the driving forces of this process are image forces and line tension. It is also expected that dislocations inside the crystals can move under the elastic interaction forces between dislocations at fairly high temperatures, overcoming the Peierls–Nabarro barrier. These movements of dislocations under the elastic interaction forces are the unique ones which take place at a much lower stress level than in the previous dislocation–velocity measurements. Because of this dislocation motion, the shape of dislocation half-loops is considered to change gradually with increasing annealing temperature so as to balance the interaction force between dislocations with the friction force acting on these dislocations.

On the other hand, silicon crystal used in device technology is usually grown in a dislocation-free state. However, dislocations are often introduced into crystals during thermal processing, which lead to a deterioration of device properties. In order to

0022–2461/84 $03.00 + .12

consider successful counterplans for controlling the nucleation of dislocations, it is necessary to recognize not only the behaviour of nucleated dislocations during heat treatment but also the stress above which dislocations begin to move at elevated temperatures.

It is desirable that observations of dislocation behaviour are performed in a thick specimen since near the surface image forces are supposed to affect the dislocation motion. By using the recently developed ultra-high intensity X-ray generator, it is now possible to follow the dynamic phenomena occurring in bulky crystals by means of *in situ* X-ray topographic observations. The purpose of the present study is to investigate the motion of individual dislocations in silicon crystals during annealing, using such a technique. From the changes in dislocation configurations at elevated temperatures, the friction forces acting on respective dislocation segments are estimated as a function of annealing temperature.

2. Experimental procedures

2.1. Specimen preparation

Specimens were prepared from dislocation-free silicon single crystals (n-type, 1.3×10^3 ohm cm) grown by the floating-zone technique. Shoulder-type specimens, as shown in Fig. 1, were prepared with a wire-abraser saw. These specimens had a gauge length of 15 mm, a width of 4 mm and a thickness of 1 mm: tensile axis parallel to $[1\bar{1}0]$ and surface orientation parallel to (1 1 2). Each specimen was mechanically polished and then the surface damaged layers were removed by chemical polishing: the final thickness of specimens was 0.7 to 0.8 mm.

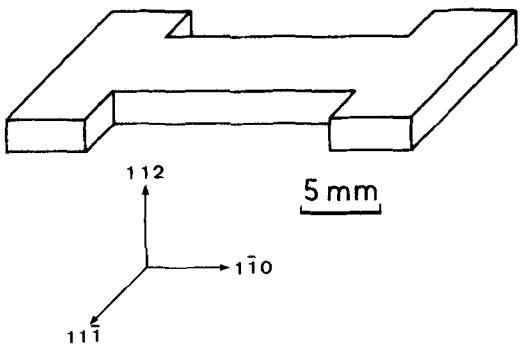

Figure 1 Shape and geometry of tensile specimen.

2.2. Introduction of isolated dislocation half-loops

The preferential nucleation sites for dislocations were introduced intentionally by scratching the (1 1 2) surface with a diamond needle, the line direction of which is perpendicular to the direction of the trace of $(1\bar{1}1)$ planes. The scratched specimens were held at 1023 K under an applied stress of about 2.5 MN m^{-2} for 10 min, so that many dislocation half-loops were nucleated at the scratch. At this stage, however, the density of dislocations in the vicinity of the scratch was too high for the individual dislocations to be resolved on an X-ray topograph. Therefore, the scratch was polished off completely after cooling by chemical polishing to reduce the dislocation density. The specimens, having isolated dislocation half-loops, were again loaded at 1073 K under an applied stress between 1.0 to 4.0 MN m^{-2} and held for 10 min under each stress to permit the isolated dislocation half-loops to expand to such an extent that they could be resolved by X-ray topography.

2.3. *In situ* X-ray topographic observations

The motion of isolated dislocation half-loops during annealing at elevated temperatures was observed *in situ* using the specimen heating apparatus [12], installed on a high-power X-ray diffraction topographic system which consisted of a 90 kW class ultra-high intensity X-ray generator (Rigaku, RU-1500), a large topographic goniometer and a TV imaging system. The specimens were annealed stepwise between 1173 and 1273 K in vacuum of about 10^{-4} torr: they were annealed for 30 min at each temperature. Ag$K\alpha_1$ radiation was used for the topography under the operating condition of 50 kV and 1200 mA and symmetric 1 1 1 reflection was employed. The motion of dislocations was observed continuously on a monitor TV: to reveal the details of dislocation configurations, the images were also recorded intermittently on Ilford-L4 nuclear research plates. The exposure time for a traverse topograph was about 1 min.

3. Experimental results

3.1. Generation of isolated dislocation half-loops

Large isolated dislocation half-loops were first introduced by tensile deformation from the scratch made on the surface. Figs. 2a and b show the topographs taken at room temperature on the

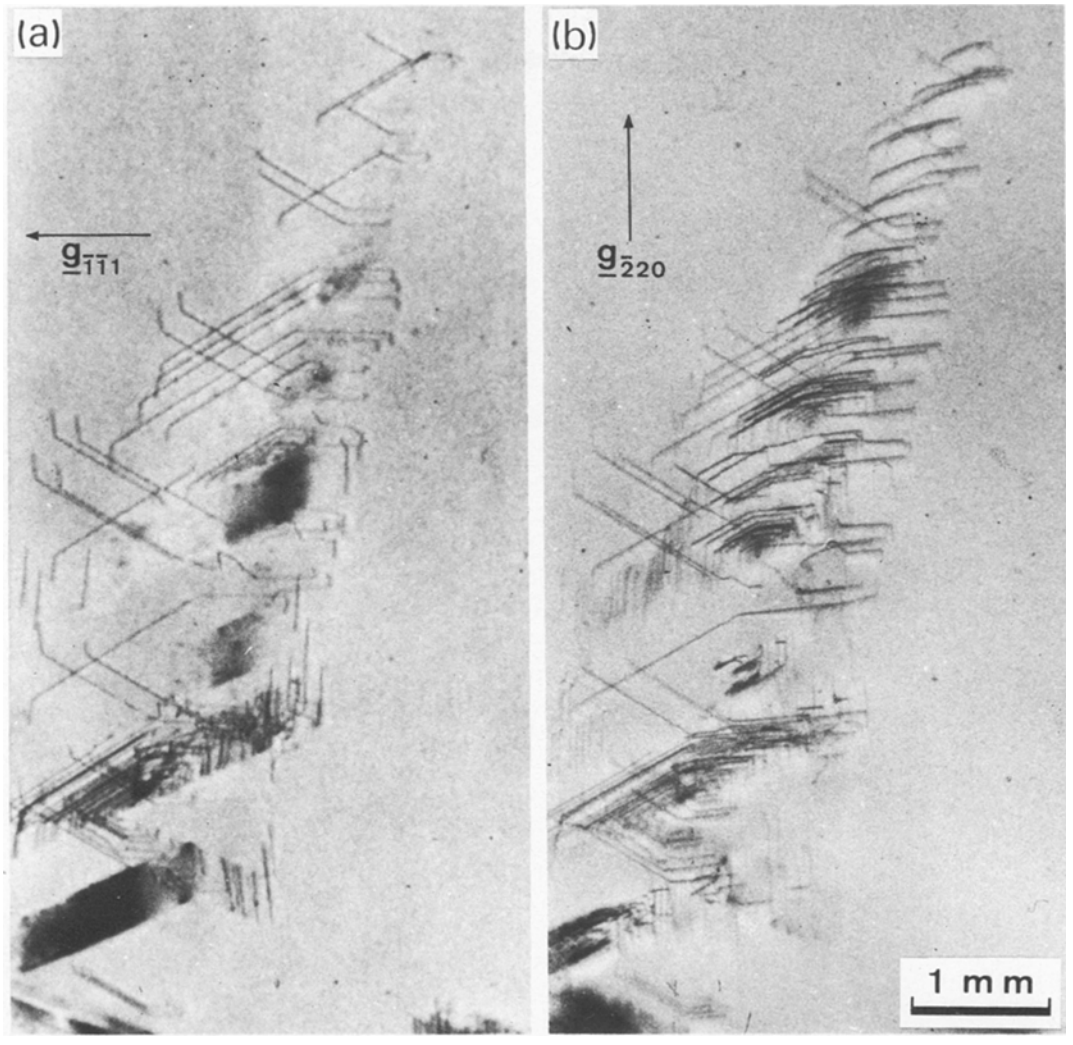

Figure 2 Large isolated dislocation half-loops expanded from the scratch by tensile deformation at 1073 K. Topographs were taken at room temperature after the applied stress was increased up to 3.6 MN m^{-2} and then holding there for 10 min; (a) $\bar{1}\bar{1}1$ reflection, (b) $\bar{2}20$ reflection.

specimen stressed up to 3.6 MN m^{-2} for 10 min at 1073 K. The dislocation half-loops consist of four straight segments lying along the ⟨1 1 0⟩ directions and the maximum loop diameter is about 2 mm in this case. Contrast experiments and trace analysis showed that dislocations generated from the scratch mostly belong to either the $[0\bar{1}1]/(\bar{1}11)$ slip system or the $[10\bar{1}]/(1\bar{1}1)$ slip system.

3.2. Motion of isolated dislocations during annealing

The specimens, in which isolated dislocation loops were introduced at 1073 K, were again heated to a temperature between 1173 and 1273 K and the changes in dislocation configurations during annealing were observed continuously, as shown in Fig. 3. Fig. 3a is the topography taken at room temperature before heating. As was found in Fig. 2, large dislocation loops which assume a half-hexagonal shape were observed. The specimen was heated to 1173 K at a heating rate of about 100 K min^{-1} and held at that temperature for 30 min (b), and then at 1223 K for an additional 30 min (c). The specimen was subsequently heated to 1273 K and held there for 10 min (d), 20 min (e) and 30 min (f).

In the as-deformed state (a), each dislocation segment was straight and strictly parallel to the ⟨1 1 0⟩ direction since the Peierls–Nabarro barrier

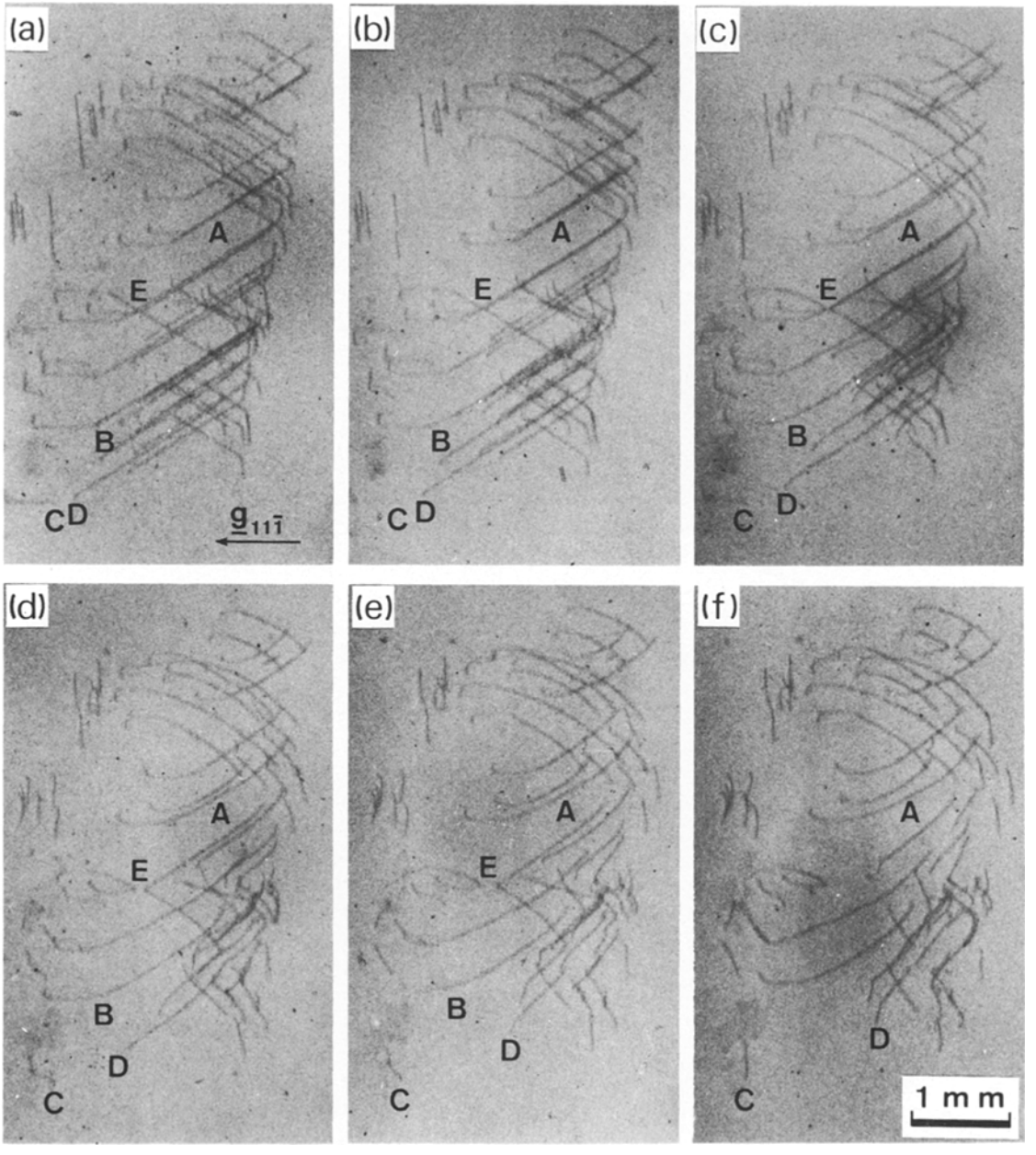

Figure 3 Evolution of dislocation configurations during annealing. (a) The topograph taken at room temperature before heating. The specimen was held at 1173 K for 30 min (b), at 1223 K for 30 min (c), and then at 1273 K for 10 min (d), 20 min (e), and 30 min (f): $11\bar{1}$ reflection.

is extremely large. That is to say, these dislocations are not in the elastically-equilibrium positions. When annealed at high temperatures, therefore, the dislocation segments were displaced to the elastically-equilibrium positions since the friction force due to the Peierls–Nabarro barrier is lowered at elevated temperatures. The noticeable features in dislocation movements during annealing are summarized as follows.

1. Repulsive interaction between parallel screw dislocations with the same sign can be seen at A. As a result, the distance between two dislocations became longer at higher annealing temperature.

2. Displacements in the position of the portion

corresponding to one of the vertices of a hexagonal loop can be seen at B. This portion is referred to as the dislocation bend [13] in the following. That is, the sharp dislocation bend turned into the gradually curved bend.

3. Movement of dislocations, which are intersected with the surface, can be seen at C and D, where the 60° segment terminated at the surface at the point A and the screw segment at B since the portion corresponding to the vertex of the hexagonal loop slipped out of the crystal during tensile deformation. Both the 60° and the screw segments emerging at the surface moved gradually during annealing and eventually they intersected with the surface prependicularly.

4. Attractive reaction between dislocations on a non-parallel slip plane can be seen at E, and this reaction leads to the formation of Lomer dislocations.

3.3. Estimation of friction force as a function of temperature

As was observed in Fig. 3, isolated dislocations moved during annealing at elevated temperatures under the influences of the elastic interaction between dislocations and of the line tension. However, the friction force acting on these dislocations prevents the aforementioned motion of dislocations, and consequently the dislocation segments assume an equilibrium position at each temperature so as to balance the friction force with the interaction force between dislocations, and the force due to line tension. Accordingly, it is possible to estimate the friction force from the configurational changes of dislocations during annealing.

In this section, the friction forces are determined as a function of annealing temperature by estimating (i) the repulsive interaction forces between the parallel screw dislocations with the same sign, and (ii) the force due to line tension for the curved dislocation near the dislocation bend.

3.3.1. Estimation of friction force from repulsive interaction between parallel dislocations with the same sign

Figs. 4a, b and c show topographs of the specimen which was annealed stepwise at 1173 K for 30 min (a), at 1223 K for 30 min (b), and at 1273 K for 10 min (c), respectively. It can be seen that the repulsive interaction between two parallel screw dislocations was realized with increasing annealing temperature, as indicated by the white arrows. Fig. 4d is a schematic illustration of Fig. 4c. From the trace analysis, as shown by the dotted line, it is found that the distance between the two slip planes, on which the two dislocation half-loops lie, is extremely small since the surface traces of two half-loops almost coincide with each other. When two parallel screw dislocations with the same sign are on the same slip plane, the repulsive interaction force between these dislocations per unit length is given by

$$F/L = \mu b^2/2\pi\Delta d \qquad (2)$$

where Δd is the distance between the two screw dislocations, b the Burgers vector of the screw dislocations, L the length of the dislocation and μ the shear modulus. By measuring the distance Δd at each annealing temperature, the repulsive interaction force between the two screw dislocations are estimated from Equation 2 as a function of annealing temperature. Although the two screw dislocations repel each other due to this interaction force, the friction force acts so as to prevent this repulsive motion of dislocations. In a state of equilibrium at each temperature, the repulsive interaction force between two screw dislocations is balanced with the friction force acting on each of them. Here, it should be noticed that near one of the surfaces the dislocation may receive the effects of image forces with the increase in the distance Δd. This can be seen at A in Figs. 3e and f, where the two screw dislocations unusually repel each other with time at 1273 K. Such being the case, the measurement of the distance Δd at 1273 K was attempted on the specimen annealed for 10 min (Fig. 4c). The friction forces thus estimated will be shown collectively afterwards.

3.3.2. Estimation of friction force from configurational changes of dislocation bend

Figs. 5a, b and c show the topographs taken at 1173 K (a), 1198 K (b) and 1223 K (c), respectively, each of which was observed after holding for 30 min at each temperature. In the same manner as in Fig. 3, the sharp dislocation bend turned into the gradually curved bend with the increase in annealing temperature, as indicated by the white arrows. Fig. 5d is a schematic illustration of Fig. 5c and represents the

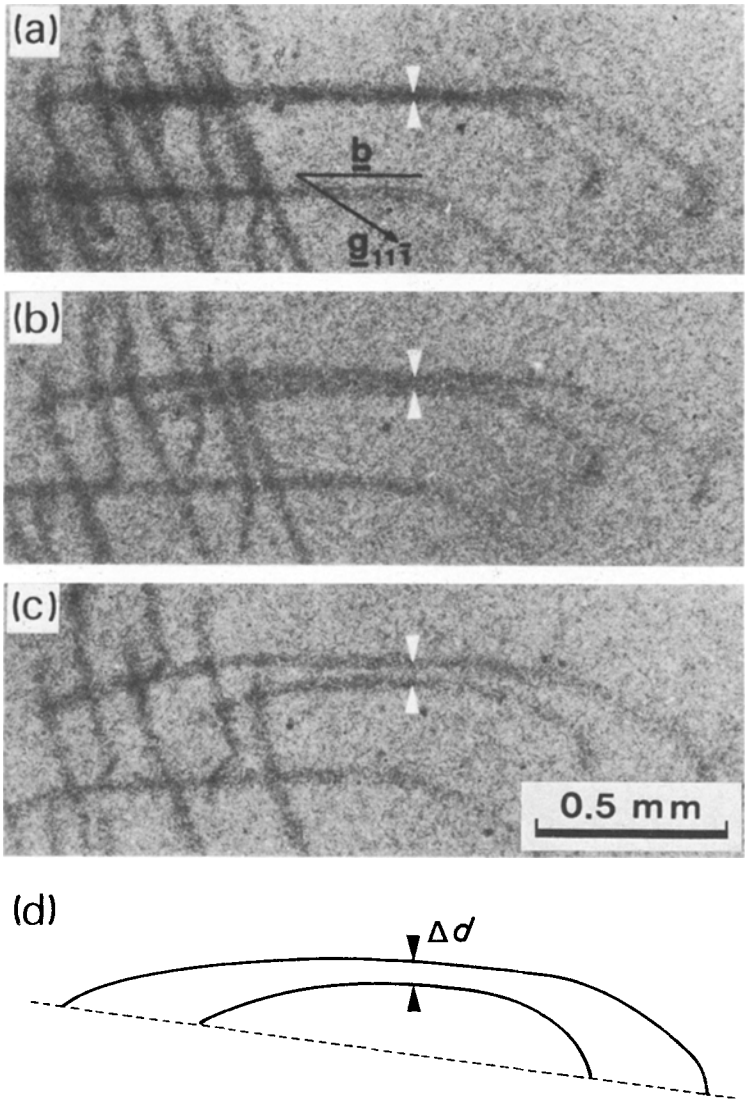

Figure 4 Repulsive interaction between parallel screw dislocations with the same sign. Topographs of the specimen annealed stepwise at 1173 K for 30 min (a), at 1223 K for 30 min (b), and at 1273 K for 10 min (c); $11\bar{1}$ reflection. **b** is the Burgers vector. Each set of white arrows indicates the distance Δd between two dislocations. Schematic illustration of (c) is shown in (d); the dotted line represents the surface trace.

equilibrium configuration of the dislocation bend changed from the position drawn by a straight broken line to that drawn by a curved solid line after this annealing. Namely, the curvature of the bend became smaller for higher temperature.

Here, it would be convenient to analyse the angular dislocation shown by a broken line in Fig. 6, since each of the straight line segments (1) and (2) is strictly parallel to the ⟨1 1 0⟩ direction before annealing. The dislocation is considered to be a smooth flexible string with a line tension. By heating the specimen, therefore, the dislocation segments near the bend move to adjust their positions so as to straighten themselves out under the influence of their line tensions. The simple line-tension analogy [14] yields

$$T = \frac{\mu b^2}{4\pi(1-\nu)}\left[(1+\nu)\cos^2\theta + (1-2\nu)\sin^2\theta\right]\ln\frac{R}{r_0} \quad (3)$$

where θ is the angle between the dislocation line and the Burgers vector, R the radius of curvature of the curved dislocation, r_0 the radius of the dislocation core, and ν the Poisson ratio. Granting that $\ln(R/r_0)$ does not differ considerably from 4π in Equation 3, for the initially screw dislocation,

$$T = \frac{1+\nu}{1-\nu}\mu b^2 \quad (4)$$

and for the initially 60° dislocation,

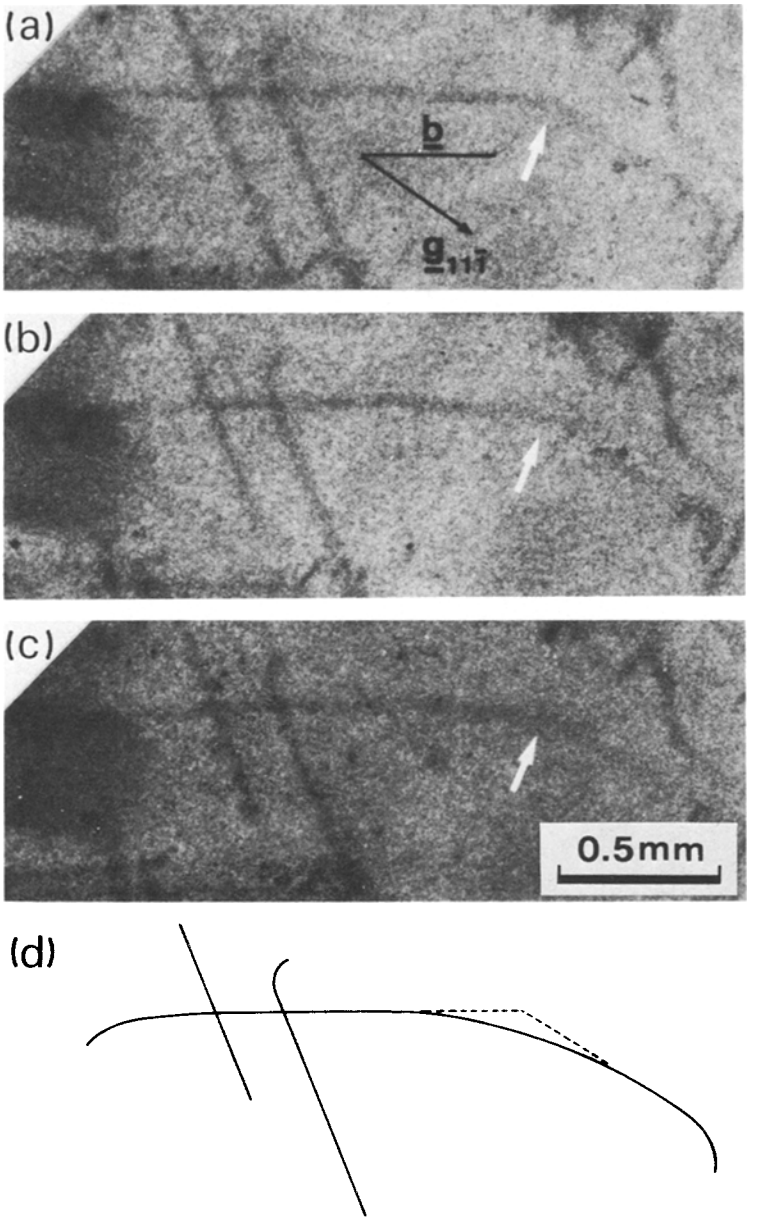

Figure 5 Configurational change of dislocation bend during annealing. Topographs were taken at 1173 K (a), 1198 K (b), and 1223 K (c), respectively, each of which was observed after holding for 30 min at each temperature; $11\bar{1}$ reflection. The white arrows indicate the dislocation bend and **b** is the Burgers vector. Schematic illustration of (c) is shown in (d): broken line and solid line represent the position of the dislocation before and after annealing, respectively.

$$T = \frac{4-5\nu}{4(1-\nu)}\mu b^2 \qquad (5)$$

As shown schematically in Fig. 6, when the distance l is a length from the bend A to the point B at which the displacement of the segment (1) is ended, the radius of curvature, R, for the originally straight line segment (1) can be determined geometrically and is equal to $3^{1/2}l$. It is found that the radius of curvature thus determined is accurate at least for the segment near the point B. Then, for the curved dislocation with the radius of curvature, $R(=3^{1/2}l)$, the force per unit length on the dislocation due to the line tension is given by

$$F/L = T/3^{1/2}l \qquad (6)$$

This force acts perpendicular to the dislocation line in a direction tending to eliminate the curvature. However, since the friction force acts so as to prevent this dislocation motion, the dislocation segments near the bend assume the equilibrium configuration after annealing at each temperature. That is to say, the force due to the line tension for the curvature $1/R$ is now equal to the friction force acting on the segment (1).

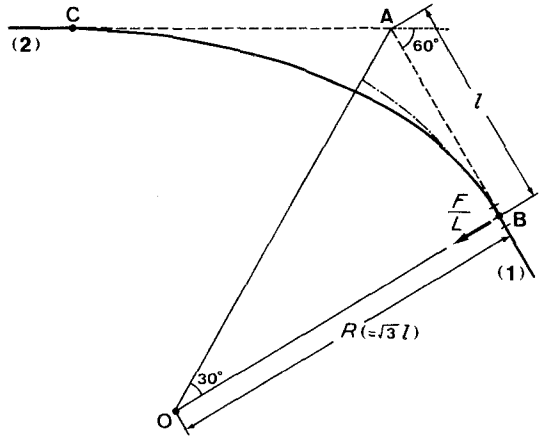

Figure 6 Schematic diagram showing dislocation bend of an angle of 60°. The broken line and solid lines represent the position of the dislocation before and after annealing, respectively. The curved dislocation near the point B is approximated by a circle with the radius of curvature, $R = 3^{1/2}l$, as shown by a chained line.

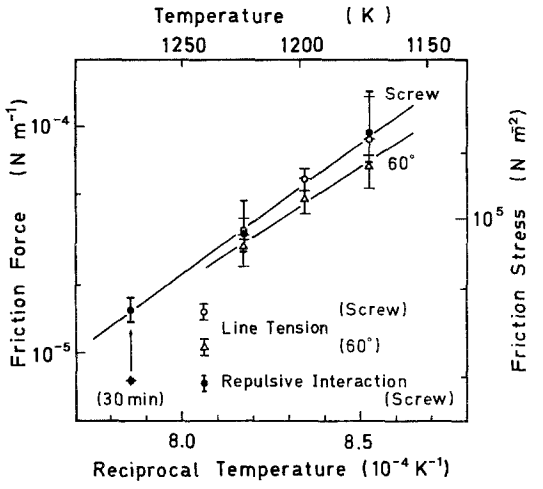

Figure 7 Friction force acting on screw and 60° dislocations as a function of annealing temperature. Friction forces are determined by estimating (i) the repulsive interaction force between parallel dislocations with the same sign, and (ii) the force due to line tension for a curved dislocation. Friction force divided by the magnitude of the Burgers vector gives friction stress.

The energy which is supplied by thermal fluctuations to overcome the Peierls–Nabarro barrier would increase in proportion to the increase in annealing temperature. As the dislocation bend turns into a curved one with, increasing temperature, the distance l also increases together. By measuring the distance l, the friction force for both screw and 60° dislocations can be estimated at each temperature using Equations 4 to 6. Fig. 7 shows the relation between the friction force acting on dislocations and the annealing temperature for both screw and 60° dislocations. The friction forces estimated in Section 3.3.1. are also included together in this figure. Each circle represents the experimental value averaged over six measurements and the vertical line attached to each circle represents the scatter range of the observed values. It is found from this figure that the friction force decreases exponentially as the annealing temperature is increased.

4. Discussion

4.1. Annealing effects on the motion of isolated dislocations

On the basis of the observations mentioned in Section 3.2 and 3.3, two effects on the motion of individual dislocations can be expected during annealing: one is due to elastic interaction forces between dislocations and the other due to line tension. As a result, the dislocation loop of half-hexagonal shape before heating changes to that of half-elliptic shape with the increase in annealing temperature, as observed in Figs. 3 to 5. In these observations, the specimen was annealed for 30 min at each temperature and then a traverse topography was taken at the same temperature to reveal the changes in dislocation configurations: at 1273 K, however, the measurement was attempted on the specimen annealed for 10 min. The displacements of dislocations during exposure were negligible in most cases. Accordingly, the annealing time settled in the annealing experiments is considered to be sufficient to reach the equilibrium configurations of dislocations at each temperature.

It has been shown that from the changes in dislocation configurations the friction force acting on dislocations can be determined by estimating the repulsive interaction force between dislocations, and the force due to the line tension. In Section 3.3, the friction force has been estimated as a function of temperature by two procedures: one is based on the repulsive interaction between parallel dislocations with the same sign (see Fig. 4) and the other the configurational change of the dislocation bend (see Fig. 5). Although these measurements have been performed independently, the magnitudes of the friction forces acting on screw dislocations obtained by these two procedures coincide well with each other at each temperature, as shown in Fig. 7. The friction forces determined from the repulsive interaction are

expected to be more accurate on the magnitudes of interaction force since the procedure is very simple and direct. On the other hand, the differences in friction force between screw and 60° dislocations are known from the measurements based on the configurational changes of dislocation bend. Still, one can recognize that dislocations in silicon crystals are movable under the lower stress than expected in spite of the extremely large Peierls–Nabbaro barrier at lower temperature.

4.2. Analysis of the temperature dependence of friction force

From Fig. 7, it is realized that the observations of dislocation motion in this case have been carried out in much lower stress range, i.e. the order of magnitude 10^{-1} MN m^{-2}, than that covered by the conventional measurements of dislocation velocity. The *in situ* X-ray topographic observations have suggested that isolated dislocations move even under fairly low stress and this movement follows the velocity equation given in Equation 1. Now, Equation 1 is used for analysing the observed results. It is also considered to be reasonable to conduct the analysis by taking $m = 1$ since the value of m in Equation 1 is almost equal to a unity for both screw and 60° dislocations. Furthermore, the dislocation density observed in Section 3.2 is extremely low, so that a one-dislocation approximation can be employed in the following.

Namely, the mean velocity $\bar{v}$ of mobile dislocations is given by

$$\bar{v} = B_0 \tau_{\text{eff}} \exp(-E/kT) \qquad (7)$$

where τ_{eff} is the effective stress. It is noted that the friction stress estimated in Section 3.3 corresponds to this effective stress. The maximum dislocation velocity in this case is considered to be obtained from the segment near the dislocation bend. This velocity was measured in Fig. 5 to be 1.8×10^{-6} cm sec^{-1} on average and almost constant at any temperature examined, but it decreased with annealing time as the dislocation segment approached its equilibrium position. Whereas, the velocity of the segment far from the bend would be much lower than that of the segment near the bend and may be approximately the same at each temperature. Accordingly, it is natural to consider that as for the segment near the point where the dislocation displacement is ended, the mean velocity $\bar{v}$ is constant at each annealing temperature and the following relation is derived from Equation 7:

$$\ln \tau = (E/kT) + C_0$$

$$C_0 = \ln \bar{v} - \ln B_0 \qquad (8)$$

where τ is the friction stress given in Fig. 7. It can be found from this relation that the temperature dependence of the friction force yields the activation energy E for dislocation motion. The activation energy is the slope of the curve shown in Fig. 7, which gives 2.4 eV for a screw dislocation and 2.2 eV for a 60° dislocation. It should be noticed that these values of activation energy have been evaluated from the analysis in the extremely low stress range where the velocity measurements are almost impossible. Neverthless, they are in good agreement with the activation energies determined in the dislocation–velocity measurements by *in situ* X-ray topography [7, 8].

Acknowledgement

The authors are grateful to Mr K. Yasuda for his assistance in operating the ultra-high intensity X-ray generator (RU-1500).

References

1. H. ALEXANDER and P. HAASEN, *Solid State Phys.* **22** (1968) 28.
2. V. C. KANNAN and J. WASHBURN, *J. Appl. Phys.* **41** (1970) 3589.
3. V. N. EROFEEV and V. I. NIKITENKO, *Sov. Phys. -JETP* **33** (1971) 963.
4. A. GEORGE, C. ESCARAVAGE, G. CHAMPIER and W. SCHRÖTER, *Phys. Status Solidi (b)* **53** (1972) 483.
5. A. FISHER, *Expr. Tech. Phys.* **23** (1975) 617.
6. S. B. KULKARNI and W. S. WILLIAMS, *J. Appl. Phys.* **47** (1976) 4318.
7. K. SUMINO, H. HARADA and I. YONENAGA, *Jpn. J. Appl. Phys.* **19** (1980) L49.
8. K. SUMINO, "Semiconductor Silicon 1981" (Electrochemical Society, Pennington, 1981) p. 208.
9. S. SCHÄFER, *Phys. Status Solidi* **19** (1967) 197.
10. H. SCHAUMBURG, *Phil. Mag.* **25** (1972) 1427.
11. H.-J. MÖLLER, *Acta Metall.* **27** (1979) 1355.
12. Y. NISHINO, M. SUZUKI, T. TONO, H. SAKA and T. IMURA, *Jpn. J. Appl. Phys.* **20** (1981) 1533.
13. J. P. HIRTH and J. LOTHE, "Theory of Dislocations", 2nd edn (John Wiley and Sons, New York, 1982) p. 136.
14. *Idem, ibid.* p. 174.

Received 7 April
and accepted 13 May 1983